Structural investigations of magnesium silicate glasses by Si-29 2D Magic-Angle Flipping NMR

ARTICLE *in* JOURNAL OF NON-CRYSTALLINE SOLIDS · JULY 2011

Impact Factor: 1.77 · DOI: 10.1016/j.jnoncrysol.2011.02.045

Journal of Non-Crystalline Solids 357 (2011) 2787–2795

Contents lists available at ScienceDirect

Journal of Non-Crystalline Solids

journal homepage: www.elsevier.com/ locate/ jnoncrysol

Structural investigations of magnesium silicate glasses by ^{29}Si 2D Magic-Angle Flipping NMR

Michael C. Davis [a,*], Kevin J. Sanders [a], Philip J. Grandinetti [a], Sarah J. Gaudio [b], Sabyasachi Sen [b]

[a] Department of Chemistry, The Ohio State University, 120W. 18th Avenue, Columbus, OH 43210-1173, United States
[b] Department of Chemical Engineering and Materials Science, University of California at Davis, Davis, CA 95616, United States

ARTICLE INFO

Article history:
Received 1 December 2010
Received in revised form 21 February 2011
Available online 1 April 2011

Keywords:
Glass;
^{29}Si NMR;
MAF;
Alkaline earth silicate;
Silicate disproportionation

ABSTRACT

The two-dimensional Magic Angle Flipping Nuclear Magnetic Resonance (2D MAF NMR) experiment on ^{29}Si nuclei is used to determine the distribution of $Q^{(n)}$ sites in two ^{29}Si-enriched magnesium silicate glasses with compositions $2MgO \cdot SiO_2$ and $MgO \cdot SiO_2$. A significant degree of polymerization is observed in the $2MgO \cdot SiO_2$ glass, supporting previous studies using Raman and ^{29}Si NMR spectroscopy. Relative abundances of 0.629 ± 0.001 for $Q^{(0)}$ and 0.371 ± 0.001 for $Q^{(1)}$ were obtained from spectral fits of the 2D MAF spectrum of the $2MgO \cdot SiO_2$ glass. Mole fractions for the free oxygen anion and each $Q^{(n)}$-species were calculated and used in a thermodynamic model of $Q^{(n)}$ disproportionation to calculate an equilibrium constant of $k_0 = 0.04 \pm 0.02$ in $2MgO \cdot SiO_2$. In the $MgO \cdot SiO_2$ glass relative abundance of 0.014 ± 0.001 for $Q^{(0)}$, 0.191 ± 0.003 for $Q^{(1)}$, 0.530 ± 0.004 for $Q^{(2)}$, 0.252 ± 0.003 for $Q^{(3)}$, and 0.014 ± 0.001 for $Q^{(4)}$ were measured. The mole fractions for the free oxygen anion and each $Q^{(n)}$-species in $MgO \cdot SiO_2$ were used to calculate corresponding disproportionation equilibrium constants of $k_1 = 0.19 \pm 0.02$, $k_2 = 0.174 \pm 0.009$, and $k_3 = 0.11 \pm 0.01$. A comparison of k_3 values from previous MAF studies of various alkali and alkaline earth silicate glasses indicate an exponential increase in k_3 with the increasing modifying cation potential. Using the van't Hoff relation, we show that differences in both thermal history and modifier cation potential contribute to this spread in k_3 values. Nuclear shielding tensor anisotropy, ζ, and asymmetry, η, values of $\zeta = 0.0$ ppm and $\eta = 0.0$ for $Q^{(0)}$ and $\zeta = 33.0 \pm 0.1$ ppm, and $\eta = 0.4 \pm 0.1$ for $Q^{(1)}$ in $2MgO \cdot SiO_2$ glass were determined from its 2D MAF spectrum. These values were used in obtaining the remaining values of $\zeta = -36.0 \pm 0.5$ ppm and $\eta = 0.99 \pm 0.01$ for $Q^{(2)}$, and $\zeta = -27.5 \pm 0.5$ ppm and $\eta = 0.45 \pm 0.11$ for $Q^{(3)}$, $\zeta = 0.0$ ppm and $\eta = 0.0$ for $Q^{(4)}$ in the $MgO \cdot SiO_2$ glass from its 2D MAF spectrum. The magnitude of ζ values observed are lower than those reported in previous MAF studies of alkali and alkaline earth silicate glasses containing different modifier cations, consistent with previously reported trends in ζ versus modifying cation potential.

1. Introduction

The atomic level ordering of silicate melts dictate their bulk thermodynamic and transport properties such as heat capacity, thermal conductivity, and viscosity [1–3]. Structurally, silicate melts are composed of a network of silicate tetrahedra that are interlinked through oxygen bonds [4]. As network modifying cations are introduced into the melt, Si—O—Si bonds are broken and non-bridging oxygen (NBO) sites are formed. Silicate melts quenched as glasses can be studied at room temperature, since the structure of the melt is preserved at the glass transition temperature. In a glass with composition $\alpha MO \cdot (1-\alpha)SiO_2$, we will assume that the following anionic equilibria [5,6] take place in the melt:

$$2Q^{(n)} \rightleftharpoons Q^{(n-1)} + Q^{(n+1)}, \tag{1}$$

and

$$2Q^{(0)} \rightleftharpoons 2Q^{(1)} + (O)^{2-}, \tag{2}$$

where $(O)^{2-}$ refers to the "free oxygen anion", which refers to OMg_n groups, i.e., oxygen not bound to silicon, and $Q^{(n)}$ refers to a silicate tetrahedron where n is the number of bridging Si—O—Si linkages per tetrahedral unit with n ranging from 0 to 4. Calculating the corresponding equilibrium constants,

$$k_n = \frac{x_{Q_{n+1}} x_{Q_{n-1}}}{\left(x_{Q_n}\right)^2}, \tag{3}$$

and

$$k_0 = \frac{\left(x_{Q_1}\right)^2 \cdot x_{(O)^{2-}}}{\left(x_{Q_0}\right)^2}. \tag{4}$$

* Corresponding author. Tel.: +614 292 8064; fax: +614 292 0559.
E-mail address: mdavis@chemistry.ohio-state.edu (M.C. Davis).

0022-3093/$ – see front matter © 2011 Elsevier B.V. All rights reserved.
doi:10.1016/j.jnoncrysol.2011.02.045

where $x_{(O)^{2-}}$ is the mole fraction of free oxygen anion and x_{Q_n} is the mole fraction of the $Q^{(n)}$ species, one can infer how the $Q^{(n)}$ anions are distributed in the bulk glass. When k_n is zero the distribution of silicate tetrahedra within the glass is binary, that is, the glass contains a maximum of two $Q^{(n)}$-species with the sequential appearance of other $Q^{(n)}$-species as the modifier cation content increases [4]. In contrast, calculated values of k_n assuming a statistically random distribution, neglecting the formation of free oxygen anion, would give $k_1 = 0.311$, $k_2 = 0.439$, and $k_3 = 0.375$ [7]. Thus, one can view the equilibrium constants as a measure of frozen-in disorder or configurational entropy of the glass.

While other analytical techniques, notably Raman spectroscopy [3], have been used to quantify $Q^{(n)}$-species in silicate glasses, NMR has been particularly useful because of the ability to elucidate short range order by distinguishing multiple sites on the basis of resonance shift [8–10]. For amorphous materials, where there is a distribution of isotropic chemical shifts for each site, lineshapes can be poorly resolved due to a large degree of overlap when multiple sites are present. Typically, multiple sites are resolved in 1D ^{29}Si MAS NMR experiments by assuming that the chemical shift distribution for each site can be represented as a Gaussian function. Areas obtained through unconstrained fitting of the 1D spectrum alone, however, cannot always be used to satisfactorily predict the necessary charge balance, and the associated uncertainty on the areas can be on the order of several percent.

Stebbins [11] showed that the markedly different ^{29}Si NMR anisotropic lineshapes of each $Q^{(n)}$-species can be exploited to detect resonances that would otherwise be strongly overlapping in the ^{29}Si MAS NMR spectrum. These anisotropic ^{29}Si lineshapes can be deconvoluted using known nuclear shielding tensor anisotropy parameters for each $Q^{(n)}$-species to determine the relative contributions from each site. This approach applied to one-dimensional static sample NMR spectra, however, is limited by low sensitivity and strong overlap of anisotropic lineshapes for different $Q^{(n)}$-species. In previous works [12–14], we demonstrated that Magic Angle Flipping (MAF) [15], which is a 2D NMR experiment capable of correlating the isotropic and anisotropic frequency contributions of the nuclear shielding along two orthogonal dimensions, provides an order of magnitude improvement in quantifying $Q^{(n)}$-species compared to fitting 1D static or MAS NMR lineshapes alone. This 2D NMR approach has been successfully applied in quantifying the relative populations of $Q^{(n)}$ in silicate glasses of composition $2Na_2O{\cdot}3SiO_2$ [12], $K_2O{\cdot}2SiO_2$ [13], and $CaO{\cdot}SiO_2$ [14].

In this work we employ 2D MAF to investigate the structure of two magnesium silicate glasses with compositions of $MgO{\cdot}SiO_2$ and $2MgO{\cdot}SiO_2$. Magnesium silicates are the primary constituents of terrestrial mantles [16]. The simplest crystalline magnesium silicate by composition is forsterite, Mg_2SiO_4, which has a single silicon site with $Q^{(0)}$ coordination [17]. In contrast, studies of forsterite ($2MgO{\cdot}SiO_2$) glass by Raman [18] and NMR [19] spectroscopy have detected multiple $Q^{(n)}$-species, indicating a significant degree of polymerization within the glass network. Similarly, in NMR studies by Sen et al. [20] on a $MgO{\cdot}SiO_2$ glass, significantly higher $Q^{(n)}$ disproportion equilibrium constants of $k_2 = 0.364$ and $k_3 = 0.464$ were observed. The objective of this work is to (1) determine the mole fractions of $Q^{(n)}$-species in each glass, (2) determine structural differences between glasses with higher MgO/SiO_2 ratios, (3) determine the degree of polymerization in the $2MgO{\cdot}SiO_2$ glass, and (4) expand on previously reported trends in both the disproportionation constant k_n and ζ with changing modifier cation potential.

2. Experimental

Samples of $\alpha MgO{\cdot}(1-\alpha)\,SiO_2$, were synthesized with 100% ^{29}Si-enriched SiO_2 using the container-less levitation technique [20]. Final spherical glass beads measured 1–2 mm in diameter. This work focuses on two compositions with $\alpha = 0.500 \pm 0.005$ and 0.660 ± 0.007, corresponding to compositions of $MgO{\cdot}SiO_2$ and $2MgO{\cdot}SiO_2$. NMR experiments were performed on a hybrid Tecmag Apollo-Chemagnetics CMX II NMR spectrometer interfaced to a 4 mm homebuilt dynamic-angle-spinning probe [21] operating at a field strength of 9.4 T, corresponding to an operating frequency of 79.476 MHz for ^{29}Si. The ^{29}Si relaxation time was measured for both glass compositions indicating a spin-lattice relaxation time, T_1, of 8 s and 26 s for $MgO{\cdot}SiO_2$ and $2MgO{\cdot}SiO_2$, respectively. The difference in T_1 between the two samples is explained by possible paramagnetic impurities that were incorporated in the glass structure during synthesis. A recycle delay of $6T_1$ was used for each glass and no changes in peak shape as a function of recycle delay were observed indicating no differential relaxation between the ^{29}Si resonances.

The 2D MAF ^{29}Si experiment correlates isotropic MAS frequencies to anisotropic frequencies obtained while spinning off the magic angle during the t_1 evolution period. Here, the off-magic angle, θ_R, is set at $\theta_R = 90^\circ$ away from the external magnetic field direction, where the averaged frequency anisotropies are scaled [22,23] by a factor of $-1/2$.

The 2D MAF spectrum of the $MgO{\cdot}SiO_2$ glass, shown in Fig. 2, was obtained using the shifted-echo MAF pulse sequence [25,26], illustrated in Fig. 1A. The number of $t_1 \times t_2$ points was 128×256 with dwell times of 62.5 μs in both dimensions. The total acquisition time was 16 days for $MgO{\cdot}SiO_2$. The 2D MAF spectrum of $2MgO{\cdot}SiO_2$ glass is shown in Fig. 3. To improve sensitivity the MAF sequence with Carr–Purcell–Meiboom–Gill (CPMG) [27,28] acquisition, illustrated in Fig. 1B, was used. The number of loops, m, in the CPMG acquisition was set to acquire 80 echoes. An echo spacing of 8 ms between π pulses was used with dwell times of 62.5 μs in t_1 and 20 μs in $t_2^{(m)}$. The use of CPMG acquisition provided a sensitivity enhancement of 4.5 over the MAF sequence of Fig. 1A. Utilizing CPMG acquisition has proven

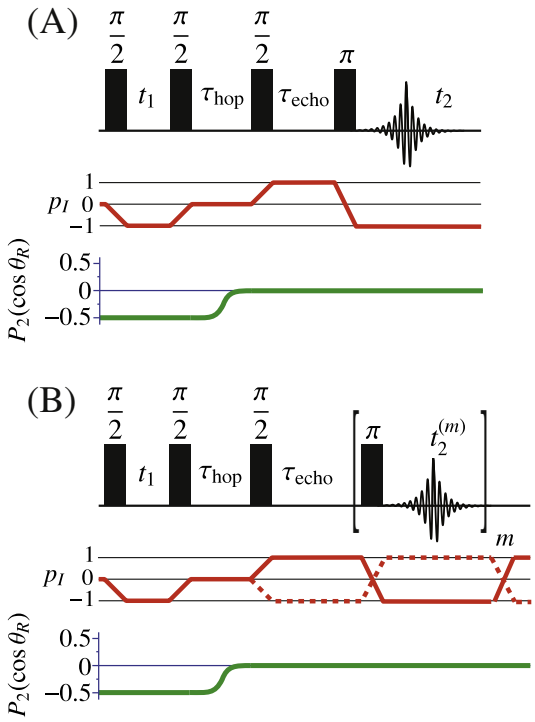

Fig. 1. (A) Shifted-echo Magic-Angle Flipping pulse sequence with spin transition and spatial symmetry pathways. (B) Magic-Angle Flipping sequence pulse using CPMG acquisition ($m = 80$) with spin and spatial symmetry pathways. In both experiments the rotor axis angle, θ_R, during t_1 is the evolution time set to $\theta_R = 90^\circ$, the period, τ_{hop}, during which the magnetization is stored as Zeeman order while the rotor is switched between angles, is set to 80 ms. The echo shift period, τ_{echo}, is set to 3.95 ms. Hypercomplex acquisition is performed to obtain positive and negative t_1 quadrants in the 2D time domain signal [24]. Four dummy scans are performed prior to acquisition to ensure that the system reached steady state prior to the start of the experiment.

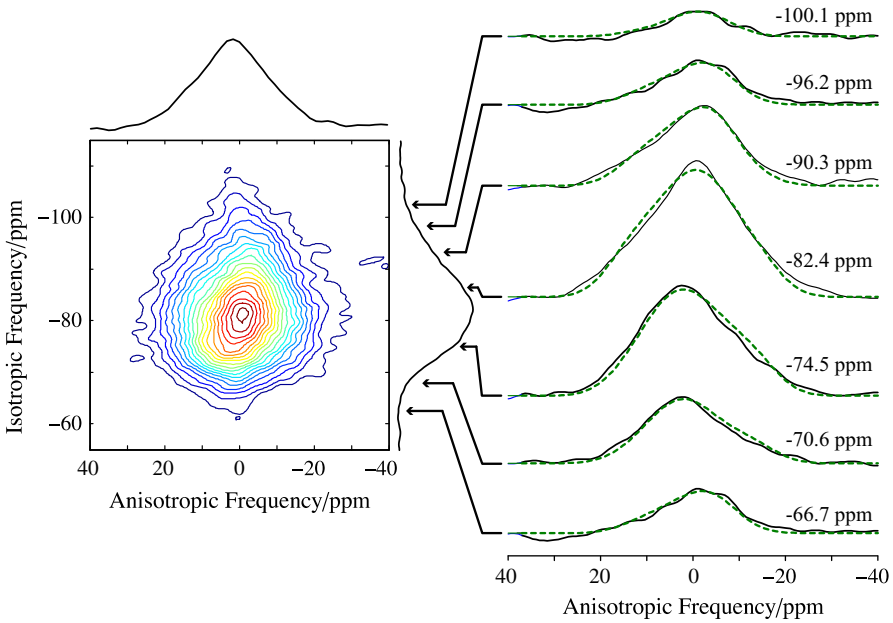

Fig. 2. Experimental 2D ^{29}Si MAF NMR spectrum of $MgO \cdot SiO_2$ with representative experimental (black lines) and simulated (green dashed lines) cross sections at selected isotropic chemical shifts ($\chi^2_{reduced} = 1.8$). All frequencies (in ppm) are referenced to TMS.

effective in analyzing both static and spinning samples because the acquisition of multiple echoes in the time domain can reduce experimental time for samples with long T_1 [29–32]. Previous studies [33,34] have already demonstrated that the acquisition dimension of other 2D correlation techniques such as Magic Angle Turning (MAT) can be enhanced by adding CPMG acquisition by increasing sensitivity. The MAF CPMG spectrum was processed using the TOP approach to CPMG as recently outlined by Dey et al. [35]. The total acquisition time was 3 days for $2MgO \cdot SiO_2$. A Gaussian apodization was applied along the anisotropic dimension with a half width at half height (HWHH) of 235 Hz to enhance the sensitivity of the 2D spectra of both samples.

As acquired, the signal from both sequences in Fig. 1 correlates a t_1 dimension containing both isotropic and anisotropic frequencies to a t_2 dimension containing only isotropic frequencies, as presented in previous MAF investigations of silicate glasses [12–14]. The 2D MAF spectra presented here, however, have been transformed to correlate a purely isotropic spectrum to a purely anisotropic spectrum through the application of an affine transformation [36], consisting of a shear parallel to t_2 using a shear factor of 1.

In this study we employ the IUPAC definitions for nuclear shielding and chemical shift interactions [37] where the isotropic nuclear shielding is defined as

$$\sigma_{iso} = \frac{1}{3}\left(\sigma_{xx} + \sigma_{yy} + \sigma_{zz}\right), \tag{5}$$

with corresponding isotropic chemical shift

$$\delta_{iso} = \frac{(\sigma_{ref} - \sigma_{iso})}{(1 - \sigma_{ref})}, \tag{6}$$

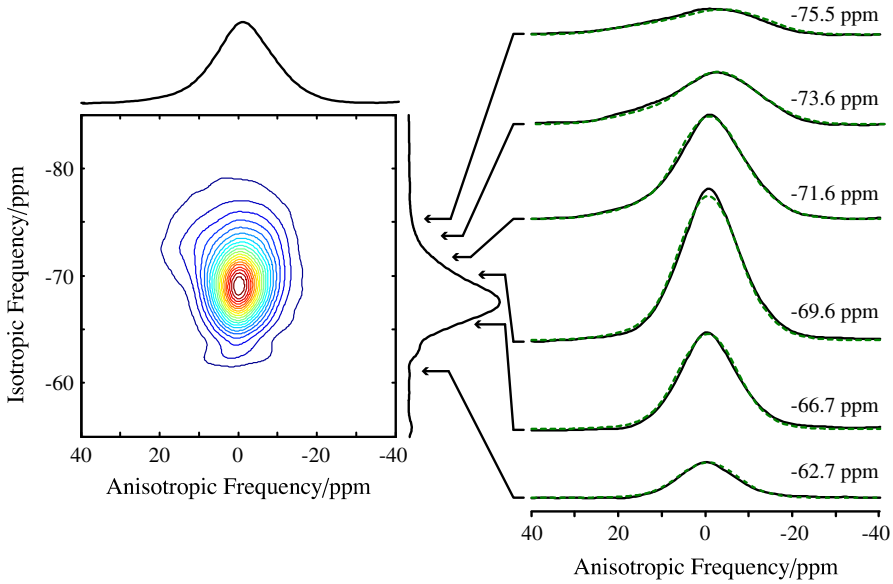

Fig. 3. ^{29}Si MAF NMR spectrum of the $2MgO \cdot SiO_2$ glass with representative experimental (black lines) and simulated (green dashed lines) cross sections at selected isotropic chemical shifts ($\chi^2_{reduced} = 1.7$). All frequencies (in ppm) are referenced to TMS.

where σ_{xx}, σ_{yy}, and σ_{zz} are the components of the nuclear shielding tensor in its principal axis system and σ_{ref} is the isotropic nuclear shielding of the reference compound (TMS). The shielding anisotropy, ζ, and asymmetry parameter, η, are defined as

$$\zeta = \sigma_{zz} - \sigma_{iso}, \tag{7}$$

and

$$\eta = \frac{\sigma_{yy} - \sigma_{xx}}{\zeta}, \tag{8}$$

respectively. Based on the results of previous MAF studies on silicate glasses [12–14], we assume that the nuclear shielding anisotropy, ζ, and asymmetry parameters, η, are identical for each $Q^{(n)}$ site. Thus, we will use the notation, $\zeta^{(n)}$ and $\eta^{(n)}$, to represent the nuclear shielding parameters for a $Q^{(n)}$ site in a magnesium silicate glass. Additionally, we assume that the distribution of isotropic chemical shifts for $Q^{(n)}$ species in the glass will be Gaussian, with a mean value, $\langle\delta_{iso}^{(n)}\rangle$. The 2D MAF spectrum was analyzed using the nonlinear least-squares fitting routine built into the Optimization toolbox of MATLAB®. The analysis incorporates the NMR simulation package SIMPSON [38] to generate an anisotropic lineshape for each $Q^{(n)}$ with a given $\zeta^{(n)}$ and $\eta^{(n)}$. Up to five anisotropic $Q^{(n)}$ lineshapes are used to generate a 2D MAF lineshape with a Gaussian distribution of isotropic chemical shifts. Thus, the parameters used to model the 2D spectrum were (1) the mean $Q^{(n)}$ isotropic chemical shift position, $\langle\delta_{iso}^{(n)}\rangle$, in the isotropic dimension, ω_2, (2) the standard deviation of each $Q^{(n)}$ isotropic chemical shift distribution in ω_2, (3) the nuclear shielding tensor anisotropy, $\zeta^{(n)}$, for each $Q^{(n)}$, (4) the nuclear shielding tensor asymmetry parameter, $\eta^{(n)}$, for each $Q^{(n)}$, (5) the integrated 2D MAF lineshape intensity for each $Q^{(n)}$, and (6) the Gaussian line broadening along ω_1, the anisotropic dimension, identical for all $Q^{(n)}$ anisotropic lineshapes.

The best-fit values for $\zeta^{(n)}$ and $\eta^{(n)}$ were determined by analyzing 1D anisotropic cross sections in the 2D MAF spectrum where each $Q^{(n)}$ dominates, and are given in Table 1 along with previously measured values. Additionally, the best-fit line broadenings obtained from the least-squares fit of the 1D anisotropic cross sections corresponded to Gaussian function with HWHH equal to 528 Hz (6.6 ppm) for both $2MgO{\cdot}SiO_2$ and $MgO{\cdot}SiO_2$. A challenge in presenting uncertainties for the shielding parameters arises from a strong covariance with the Gaussian line broadening that is also used in the least-squares analysis of anisotropic lineshapes. After subtracting the 228 Hz of Gaussian apodization applied during signal processing, only 293 Hz (3.7 ppm) of the line broadening found during least-squares analysis of the anisotropic cross sections can be attributed to structural disorder, intrinsic excited state lifetime, and uncertainty in the tensor parameters. The uncertainties in the shielding tensor, therefore, can range from values as low as those reported in Table 1 to as high as 3.7 ppm. The best fit values for the mean and standard deviation of each $Q^{(n)}$ isotropic chemical shift distribution, as well as the integrated intensity for each $Q^{(n)}$ were determined by analyzing the full 2D MAF spectrum, and are given in Table 2.

To calculate the equilibrium constants of Eqs. (3) and (4) one needs the $(O)^{2-}$ mole fraction,

$$x_{(O)^{2-}} = \frac{n_{(O)^{2-}}}{n_{Q_0} + n_{Q_1} + n_{Q_2} + n_{Q_3} + n_{Q_4} + n_{(O)^{2-}}}, \tag{9}$$

as well as the $Q^{(n)}$ mole fractions,

$$x_{Q_n} = \frac{n_{Q_n}}{n_{Q_0} + n_{Q_1} + n_{Q_2} + n_{Q_3} + n_{Q_4} + n_{(O)^{2-}}}, \tag{10}$$

where n_{Q_n} are the total number of moles of Q_n, and $n_{(O)^{2-}}$ is the total number of moles of the anion $(O)^{2-}$. From the analysis of our ^{29}Si NMR 2D spectra one can measure the fraction of silicon in each of the five Q_n forms, y_{Q_n}, that is,

$$y_{Q_n} = n_{Q_n} / n_{S_i}, \tag{11}$$

where n_{Q_n} is the number of moles of the species $Q^{(n)}$, and n_{Si} is the total number of mole of silicon. If the anion $(O)^{2-}$ is not present in the glass, then

$$x_{Q_n} = y_{Q_n}, \tag{12}$$

and the calculation of the $Q^{(n)}$ disproportionation constants, k_n, is straightforward. When the glass network is sufficiently depolymerized, near the orthosilicate composition, however, there may be significant $(O)^{2-}$ anion present. In this situation, Eq. (12) will no longer be valid [39–44]. Combining the relative $Q^{(n)}$ abundances of Eq. (11), obtained by ^{29}Si NMR, with the constraint of charge balance, as derived in the Appendix, the mole fractions of all species in the equilibria of Eqs. (1) and (2) are calculated according to

$$x_{(O)^{2-}} = \frac{\left(\frac{\alpha}{1-\alpha}\right) - 2y_{Q_0} - 1.5y_{Q_1} - y_{Q_2} - 0.5y_{Q_3}}{\left(\frac{\alpha}{1-\alpha}\right) - y_{Q_0} - 0.5y_{Q_1} + 0.5y_{Q_3} + y_{Q_4}}, \tag{13}$$

and

$$x_{Q_n} = \frac{y_{Q_n}}{\left(\frac{\alpha}{1-\alpha}\right) - y_{Q_0} - 0.5y_{Q_1} + 0.5y_{Q_3} + y_{Q_4}}. \tag{14}$$

Using the expressions above with the ^{29}Si NMR relative $Q^{(n)}$ abundances given in Table 2, the mole fractions, also shown in Table 2, were calculated.

3. Discussion

3.1. $2MgO{\cdot}SiO_2$

The one-dimensional ^{29}Si MAS spectrum of $2MgO{\cdot}SiO_2$ glass is shown in Fig. 4A. This spectrum has a broad resonance peaking at $\delta_{iso} = -67$ ppm, consistent with the presence of $Q^{(0)}$ species. The MAS lineshape is also skewed towards an isotropic chemical shift of −80 ppm, suggesting the presence of $Q^{(1)}$ species. A sharp low

Table 1
Nuclear shielding anisotropy parameters, $\zeta^{(n)}$ and $\eta^{(n)}$, for $Q^{(n)}$ in magnesium silicates studied in this work and compared to previous 2D ^{29}Si MAF NMR studies of other silicate glasses. Nuclear shielding parameters reported in this study were obtained from spectral fits of a 1D data slice of the MAF spectrum where the mole fraction of a particular $Q^{(n)}$ was expected to dominate. As explained in the main text the uncertainties in the shielding anisotropy can range from the values reported above to as high as 3.7 ppm.

Glass	Reference	$\zeta^{(0)}$/ppm	$\zeta^{(1)}$/ppm	$\zeta^{(2)}$/ppm	$\zeta^{(3)}$/ppm	$\zeta^{(4)}$/ppm	$\eta^{(0)}$	$\eta^{(1)}$	$\eta^{(2)}$	$\eta^{(3)}$	$\eta^{(4)}$
$K_2O{\cdot}2SiO_2$	[13]	–	–	−85.0 ± 1.3	−74.9 ± 0.2	0.0	–	–	0.48 ± 0.02	0.030 ± 0.006	0.0
$2Na_2O{\cdot}3SiO_2$	[12]	–	–	−78.0	−69	0.0	–	–	0.53	0.03	0.0
$CaO{\cdot}SiO_2$	[14]	–	40.0	−48.3	−45.4	0.0	–	0.4	0.70	0.01	0.0
$2MgO{\cdot}SiO_2$	This work	0.0	33.0 ± 0.1	–	–	–	0.0	0.4 ± 0.1	–	–	–
$MgO{\cdot}SiO_2$	This work	0.0	33.0 ± 0.1	−36.0 ± 0.5	−27.5 ± 0.5	0.0	0.0	0.4 ± 0.1	0.99 ± 0.07	0.45 ± 0.11	0.0

Table 2
Mean, standard deviation, silicon mole fraction (y_{Q_n}) and mole fraction (x) for each of the five $Q^{(n)}$ isotropic chemical shift distributions that compose the ^{29}Si MAF NMR spectra of $2MgO{\cdot}SiO_2$ and $MgO{\cdot}SiO_2$ and the calculated free oxygen anion. Values from this work are presented with previously reported values by Sen and Tangeman [19] and Sen et al. [20]. Because of the low relative area, the value of $\langle\delta_{iso}^{(4)}\rangle$, indicated with asterisks in the table, was constrained to the $\langle\delta_{iso}^{(4)}\rangle$ value reported by Sen et al. [20] to prevent the χ^2 minimization from converging on unphysical values.

$2MgO{\cdot}SiO_2$	Sen and Tangeman [19]				This work			
	$\langle\delta_{iso}^{(n)}\rangle$/ppm	Width	y_{Q_n}	x	$\langle\delta_{iso}^{(n)}\rangle$/ppm	Standard deviation/ppm	y_{Q_n}	x
$Q^{(0)}$	−66	–	0.49 ± 0.04	0.41 ± 0.05	−68.8 ± 0.1	2.55 ± 0.05	0.629 ± 0.001	0.56 ± 0.03
$Q^{(1)}$	−73	–	0.51 ± 0.04	0.43 ± 0.05	−72.5 ± 0.1	3.49 ± 0.02	0.371 ± 0.001	0.33 ± 0.02
$(O)^{2-}$	n/a	n/a	n/a	0.16 ± 0.09	n/a	n/a	n/a	0.11 ± 0.05
$MgO{\cdot}SiO_2$	Sen et al. [20]				This work			
	$\langle\delta_{iso}^{(n)}\rangle$/ppm	Width	y_{Q_n}	x	$\langle\delta_{iso}^{(n)}\rangle$/ppm	Standard deviation/ppm	y_{Q_n}	x
$Q^{(0)}$	–	–	0.0	–	−66.8 ± 0.2	3.2 ± 0.1	0.014 ± 0.001	0.014 ± 0.001
$Q^{(1)}$	−74.9	11.7	0.250	0.232	−73.5 ± 0.1	3.9 ± 0.1	0.191 ± 0.003	0.185 ± 0.004
$Q^{(2)}$	−83.9	12.6	0.420	0.390	−81.1 ± 0.1	5.3 ± 0.1	0.530 ± 0.004	0.51 ± 0.01
$Q^{(3)}$	−94.2	13.2	0.257	0.238	−90.8 ± 0.1	6.5 ± 0.1	0.252 ± 0.003	0.245 ± 0.005
$Q^{(4)}$	−107.2	14.9	0.073	0.067	−107.2*	6.0 ± 0.4	0.014 ± 0.001	0.013 ± 0.001
$(O)^{2-}$	n/a	n/a	n/a	0.071	n/a	n/a	n/a	0.03 ± 0.02

intensity peak was also observed at $\delta_{iso} = -62$ ppm in the isotropic dimension, which has been previously observed in ^{29}Si NMR investigations [19] of the same material and corresponds to a small crystalline forsterite impurity.

In recent works on $2MgO{\cdot}SiO_2$ glass by Kalampounias et al. [18] and Sen and Tangeman [19], a significant degree of polymerization was proposed to exist within magnesium silicate glasses at high magnesium concentrations, with silicon existing as $Q^{(0)}$, $Q^{(1)}$, and perhaps $Q^{(2)}$. The conclusions of Sen and Tangeman [19] were based on analyses of static ^{29}Si NMR spectra where they found two sites attributed to $Q^{(0)}$ with $\zeta^{(0)} = 0$ ppm and $\eta^{(0)} = 0.0$ and $Q^{(1)}$ with $\zeta^{(1)} = 45$ ppm and $\eta^{(1)} = 0.9$. The ^{29}Si 2D MAF spectrum of $2MgO{\cdot}SiO_2$ glass, shown in Fig. 3, reveals a broadening along the anisotropic dimension as the isotropic frequency increases from $\delta_{iso} = -62$ to -80 ppm, confirming the presence of a second site, which is consistent for silicon with $Q^{(1)}$ coordination. Analysis of the 2D MAF spectrum yields nuclear shielding parameters $\zeta^{(0)} = 0.0$ ppm, $\eta^{(0)} = 0.0$, $\zeta^{(1)} = 33.0 \pm 0.1$ ppm, and $\eta^{(1)} = 0.4 \pm 0.1$. The discrepancy with Sen and Tangeman's nuclear shielding parameters for $Q^{(1)}$ is likely due to an error in their analysis arising from the large degree of spectral overlap in the 1D static NMR lineshape. Spectral fits of the 2D MAF spectrum of $2MgO{\cdot}SiO_2$ glass were also undertaken using the $\zeta^{(1)}$ value of Sen and Tangeman [19], but the chi-squared value obtained was significantly larger than the value obtained using the shielding tensor parameters in Table 1. Because of the resolution improvement of 2D MAF over 1D static NMR experiments we believe that the tensor parameters obtained in this study are more accurate.

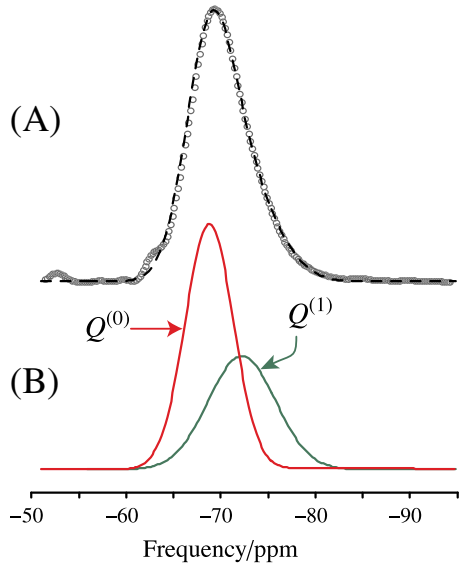

Fig. 4. Reconstructed 1D NMR lineshape from the least-squares analysis of the $2MgO{\cdot}SiO_2$ ^{29}Si MAF NMR spectrum with (A) the isotropic projection of the 2D MAF spectrum (gray circles) with the best fit (dashed line) and (B) Gaussians representing the relative areas of $Q^{(1)}$ and $Q^{(1)}$. All frequencies (in ppm) are referenced to TMS.

It is also worth noting that measurements of the nuclear shielding tensor of $Q^{(0)}$ in crystalline forsterite by Weiden and Rager [45] and Ashbrook et al. [46] gave values of $\zeta^{(0)} = -32.2$ ppm and $\eta^{(0)} = 0.51$. Given the amorphous nature of the glass, such discrepancies with shielding parameters in crystalline materials are not unexpected. In crystalline silicates, the local bonding around silicon has to fulfill long range structural order constraints, causing silicon in $Q^{(0)}$ to reside in slightly more distorted tetrahedra leading to non-zero ζ and η values. In contrast, glasses have no such long-range structural constraints, and the $Q^{(0)}$ silicon atoms tend to adopt more symmetric local structures allowing the assumption that the values of ζ and η are equal to zero as observed in previous investigations of silicate glasses by 2D MAF NMR [12–14].

Attempts were made to analyze the 2D MAF spectrum of $2MgO{\cdot}SiO_2$ glass with contributions from $Q^{(0)}$, $Q^{(1)}$, and $Q^{(2)}$ but only the inclusion of $Q^{(0)}$ and $Q^{(1)}$ gave satisfactory fits. The distributions of isotropic chemical shifts for $Q^{(0)}$ and $Q^{(1)}$ are shown in Fig. 4B. A comparison of the relative abundances of $Q^{(0)}$ and $Q^{(1)}$ to those by Sen and Tangeman [19] are also given in Table 2. As noted above, however, disagreements with Sen and Tangeman [19] arise from their use of $Q^{(1)}$ nuclear shielding parameters that were significantly larger than the true values.

Using the relative abundance of each $Q^{(n)}$-species obtained from spectral fits of the 2D MAF spectrum, given in Table 2, and Eqs. (13) and (14), the mole fractions were calculated for each $Q^{(n)}$ and $(O)^{2-}$. These results, also shown in Table 2, indicate $x_{Q_0} = 0.56 \pm 0.03$, $x_{Q_1} = 0.33 \pm 0.02$, and $x_{(O)^{2-}} = 0.11 \pm 0.05$ for the $2MgO{\cdot}SiO_2$ glass. The presence of $(O)^{2-}$ is not unreasonable given oxide ion activities determined at lower SiO_2 contents in MO–SiO_2 liquids, where M can be Mg, Fe, Ni, etc., by thermochemical means [42,47,48], although it is difficult to extrapolate such data down in temperature from the liquidus to the glass transition. Additionally, it is noteworthy that several magnesium silicates, including crystalline β-Mg_2SiO_4 [49] contain OMg_n groups.

The mole fractions were used in Eq. (4) to calculate a disproportionation constant $k_0 = 0.04 \pm 0.02$ for the $2MgO{\cdot}SiO_2$ glass. The nonzero k_0 for $2MgO{\cdot}SiO_2$ indicates a tendency for silicon to polymerize within the glass melt at large modifier cation concentrations. Of course, from charge balance alone, an increase in free oxygen anion concentration would require a decrease in the number of non-bridging oxygen in the glass structure. This k_0 value is consistent with

values of $k_0 = 0.0016$ for $CaO \cdot SiO_2$, obtained by Masson et al. [40] in applications of polymer theory to free energy of mixing data.

3.2. $MgO \cdot SiO_2$

In the 1D ^{29}Si MAS NMR spectrum of $MgO \cdot SiO_2$ shown in Fig. 6A a single broad resonance centered at −82 ppm was observed, indicative of a structure predominantly composed of $Q^{(2)}$-species. While the 1D lineshape is completely unresolved, the width and shape of the peak indicate the presence of multiple overlapping sites. Deconvoluting this lineshape, assuming the chemical shift distribution for each site is Gaussian, indicates that the spectrum is composed of five separate sites for each possible $Q^{(n)}$-species.

The 2D ^{29}Si MAF NMR spectrum of $MgO \cdot SiO_2$ is shown in Fig. 2. In a previous study of alkali silicate glasses [13], the magnitude of $\zeta^{(n)}$ for $Q^{(2)}$ and $Q^{(3)}$ was observed to be proportional to cation potential, which is defined as the charge of the cation divided by its atomic radius, for silicate glasses with different modifying cations (K^+, Na^+, Ca^{2+}, Mg^{2+}), as shown in Fig. 5, where nuclear shielding tensor parameters are given in Table 1. This trend was observed by Grimmer and coworkers [50,51]. That is, the nuclear shielding tensor along the Si–NBO bond for a $Q^{(3)}$ site decreases as the length of the Si–NBO bond approaches the length of a bridging Si—O bond. When the nuclear shielding along each bond becomes identical, the shielding anisotropy reduces to zero. This trend in nuclear shielding versus cation potential is used to explain the diminished resolution along the anisotropic dimension compared to previous MAF studies of alkali silicate glasses and the similarities between the anisotropic lineshape for each $Q^{(n)}$ species. While similar, however, distinct trends are noticeable in the 2D ^{29}Si MAF NMR spectrum of the $MgO \cdot SiO_2$ glass including a narrowing of the lineshape towards higher frequency and a shift in the symmetry of the lineshape around −80 ppm indicating multiple $Q^{(n)}$ sites with different nuclear shielding parameters arising from different bonding environments.

Analysis of the 2D MAF spectrum requires accurate values for the nuclear shielding parameters for each $Q^{(n)}$ site. Since $Q^{(0)}$ and $Q^{(4)}$ reside in a tetrahedron with uniform symmetry, the values of ζ and η for $Q^{(0)}$ and $Q^{(4)}$ can be fixed at zero. Values of $\zeta^{(1)}$ and $\eta^{(1)}$ are known from spectral fits presented earlier in this study of the $2MgO \cdot SiO_2$ and set equal to $\zeta^{(1)} = 33.0 \pm 0.1$ ppm and $\eta^{(1)} = 0.4 \pm 0.1$ leaving only $Q^{(2)}$ and $Q^{(3)}$ to be determined. These values were found by fitting respective cross sections of the 2D lineshape where those sites were believed to dominate and determined to be $\zeta^{(2)} = -36.0 \pm 0.5$ ppm, $\eta^{(2)} = 0.99 \pm 0.07$, $\zeta^{(3)} = -27.5 \pm 0.5$ ppm and $\eta^{(3)} = 0.45 \pm 0.11$. It should be noted that the $Q^{(n)}$ abundances are sensitive to the nuclear shielding parameters used to model the anisotropic dimension of the 2D MAF spectrum. Using these values for $\zeta^{(n)}$ and $\eta^{(n)}$ the entire 2D spectrum was fit to obtain relative abundance for each $Q^{(n)}$-species, as shown in Fig. 6.

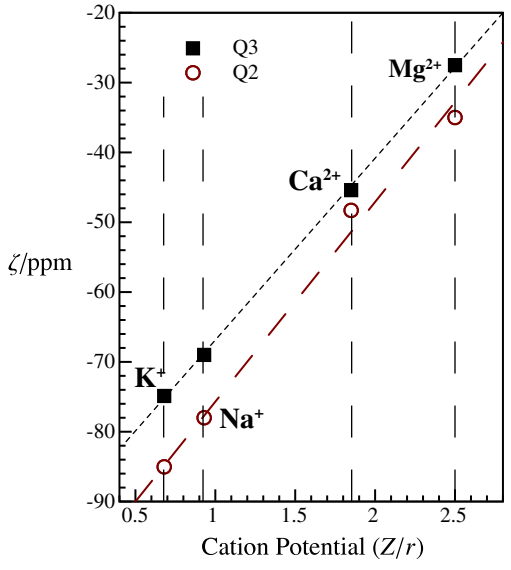

Fig. 5. Plot of ζ versus cation potential (Table 1) for $Q^{(2)}$ and $Q^{(3)}$. Values for the interatomic radium (r) were taken from work by Whittaker and Muntus [52].

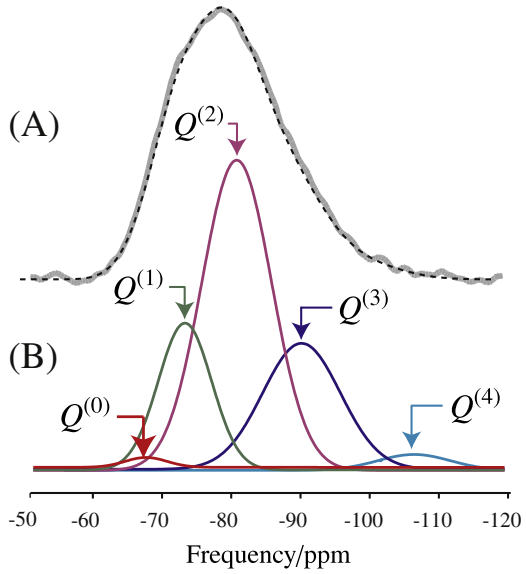

Fig. 6. Reconstructed 1D ^{29}Si MAS NMR lineshape from obtained relative areas of each $Q^{(n)}$ in the $MgO \cdot SiO_2$ glass with (A) the isotropic projection of the 2D MAF spectrum (gray line) and the least squares best fit (dashed line) and (B) Gaussians representing integrated areas for each $Q^{(n)}$ obtained from least-squares fitting of the 2D ^{29}Si MAF NMR spectrum. All frequencies (in ppm) are referenced to TMS.

Shown in Fig. 2 are selected $\theta_R = 90^\circ$ cross sections with the associated least-squares best fit simulation. The relative areas of each of the Gaussian functions projected along the isotropic dimension provide a reconstructed 1D MAS NMR lineshape with the relative area under each Gaussian corresponding to the mole fraction, given in Table 2, of each of the five $Q^{(n)}$-species. Using the relative abundance for spectral fits of the 2D MAF spectrum, the mole fraction for each $Q^{(n)}$-species and the free oxygen anion were calculated. All spectral fits are based on the assumption that the values of $\zeta^{(n)}$ and $\eta^{(n)}$ do not change as a function of the isotropic chemical shift and the chemical shift distribution is purely Gaussian. These assumptions have been used successfully in previous investigations [13] using the same analysis.

The calculated mole fractions, as reported in Table 2 for each species in the $MgO \cdot SiO_2$ glass are $x_{Q^{(0)}} = 0.014 \pm 0.001$, $x_{Q^{(1)}} = 0.185 \pm 0.004$, $x_{Q^{(2)}} = 0.51 \pm 0.01$, $x_{Q^{(3)}} = 0.245 \pm 0.005$, $x_{Q^{(4)}} = 0.013 \pm 0.001$, and $x_{(O)^{2-}} = 0.03 \pm 0.02$. These results indicate that $x_{(O)^{2-}}$ is significantly smaller than in $2MgO \cdot SiO_2$ and approximately the same as $x_{Q^{(0)}}$ within the reported uncertainty.

The mole fraction for each site was then applied to known thermodynamic disproportionation models given in Eqs. (3) and (4) to calculate equilibrium constants of $k_1 = 0.19 \pm 0.02$, $k_2 = 0.174 \pm 0.009$, and $k_3 = 0.11 \pm 0.01$. The high uncertainty in $x_{(O)^{2-}}$ precludes calculation of k_0 for this composition. The disproportionation constants k_1, k_2, and k_3 indicate a more random distribution of $Q^{(n)}$ species within the glass structure, compared to previously studied silicate glasses, as shown in Fig. 7A with values given in Table 2. These k_n values are lower than the previously reported values of $k_2 = 0.364$ and $k_3 = 0.464$ by Sen et al. [20], obtained from unconstrained fitting of 1D ^{29}Si MAS NMR lineshapes. Again, given the improved resolution of 2D MAF over 1D MAS NMR experiments, we believe that the k_n values obtained in this study are more accurate.

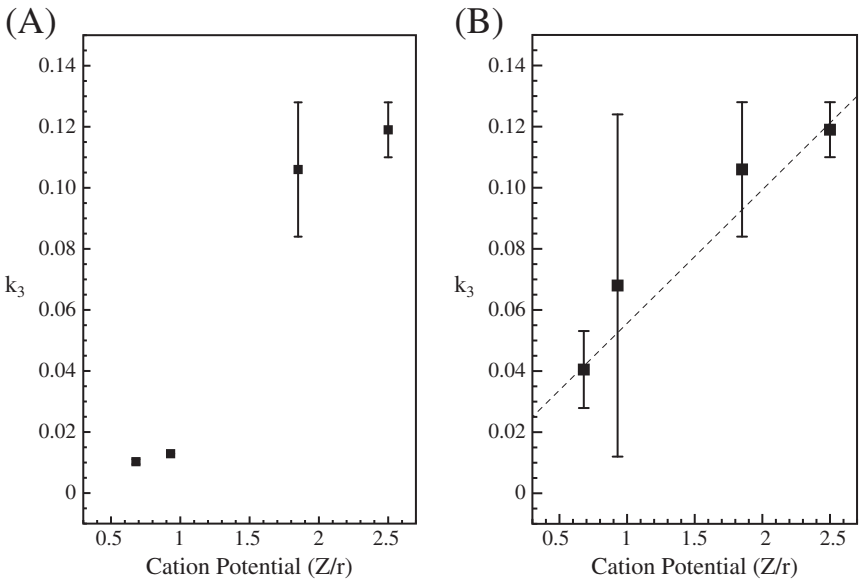

Fig. 7. (A) Dependence of k_3 on cation potential neglecting the effects of glass transition temperature where the error bars for $K_2O{\cdot}2SiO_2$ and $2Na_2O{\cdot}3SiO_2$ are on the order of the data points and (B) dependence of k_3 on cation potential using values of k_3 at a glass transition temperature of 1039 K. Dashed lines represent general trend lines and do not correspond to a specific analytical expression. Values for r were taken from work by Whittaker and Muntus [52].

3.2.1. Thermal dependence of k_n

Comparing the value of k_3 observed for the $MgO{\cdot}SiO_2$ glass to previously reported values from other ^{29}Si MAF investigations conducted in this lab and in previous studies [11,20,53–57] an exponential increase in the disproportionation constant is observed as the modifying cation potential increases, as shown in Fig. 7, consistent with observations by previous investigators [58–60]. From these results, however, it is unclear whether the increase in k_3 is purely a function of the cation potential or if the different thermal histories of the different glass compositions significantly affect k_3. Previous studies have also noted a dependence of the disproportionation constant with cooling rate [61] and Brandriss and Stebbins [58] reported a dependence of the disproportionation constant on the glass transition temperature. Brandriss and Stebbins [58] observed that as the glass transition temperature increases the disproportionation reaction given in Eq. (1) will shift to the right, causing k_n to increase.

Brandriss and Stebbins [58] used the van't Hoff equation

$$\frac{d\ln k_n}{dT} = \frac{\Delta H^\circ}{RT^2} \tag{15}$$

where k_n is the disproportionation reaction equilibrium constant, ΔH° is the standard enthalpy of the disproportionation reaction, and T is temperature, to explain the variations in the disproportionation reaction equilibrium constants observed in glasses quenched from silicate melts at different rates. In this study we use the reverse approach of Brandriss and Stebbins [58] to calculate the expected change in the disproportionation constant k_3 with glass transition temperature using standard enthalpies of the disproportionation reaction taken from Brandriss and Stebbins [58] for calcium and sodium silicate glasses and Malfait et al. [62] for the potassium disilicate glass (Table 3). Integrating Eq. (15), one obtains

$$k_n(T_2) = k_n(T_1)\exp\left[\frac{-\Delta H^\circ}{R}\left(\frac{1}{T_2}-\frac{1}{T_1}\right)\right] \tag{16}$$

where $T_1 = T_g$ of the sodium, potassium or calcium silicate glass and $T_2 = T_g$ of the magnesium silicate glass. Using Eq. (16) and values for ΔH° and the T_g values given in Table 3, k_n was calculated at the highest glass transition temperature of all the compositions compared in this study, i.e., the magnesium silicate glass, $T_g = 1039$ K. The resulting values, shown in Fig. 7B, indicate that the disproportionation constant, k_3, still increases with the cation potential even if they were measured at the same temperature, i.e., the T_g for the magnesium silicate glass. Because of the large uncertainty of ~50% on the enthalpy values reported by Brandriss and Stebbins [58] it is difficult to discern a clear trend. Nonetheless, this indicates that thermal history alone cannot account for the differences in k_3 among silicate glasses of different compositions.

4. Conclusions

We present a structural investigation of two magnesium silicate glasses with composition $2MgO{\cdot}SiO_2$ and $MgO{\cdot}SiO_2$. For the $MgO{\cdot}SiO_2$ glass we observe contributions in the ^{29}Si 2D MAF spectrum from all $Q^{(n)}$-species, whereas, for the $2MgO{\cdot}SiO_2$ glass we only observe contributions from $Q^{(0)}$ and $Q^{(1)}$, confirming observations by Sen and Tangeman [19] and Kalampounias et al. [18]. Using charge balance constraints, the presence of significant free oxygen anion, $(O)^{2-}$, was inferred in the $2MgO{\cdot}SiO_2$ glass. The presence of free oxygen anion in the $MgO{\cdot}SiO_2$ was also inferred but with significantly lower abundance than in the $2MgO{\cdot}SiO_2$ glass. Thus, from the calculated mole fractions of the $2MgO{\cdot}SiO_2$ glass the $Q^{(0)}$ disproportionation constant, k_0, for $2MgO{\cdot}SiO_2$ was obtained for the first time. While free oxygen anion is not directly observed in the ^{29}Si NMR, the predicted abundance in magnesium silicate glasses suggests that the free oxygen anion may be observable in ^{17}O solid-state NMR studies of ^{17}O-enriched silicate glasses.

Using the relative abundances of $Q^{(n)}$ measured in the ^{29}Si 2D MAF spectrum of the $MgO{\cdot}SiO_2$ glass the $Q^{(n)}$ disproportionation constants,

Table 3
Values for k_3, cation potential (Z/r), glass transition temperature (T_g), ΔH°, and the predicted k_3 value at 1039 K for glasses of different compositions. Values for ΔH° were taken from Brandriss and Stebbins [58] and Malfait et al. [62].

Glass composition	k_3	Z/r	T_g (K)	ΔH° (kJ/mol)	k_3 at 1039 K
$K_2O{\cdot}2SiO_2$	0.01029 ± 0.0008	0.68	765	33.1 ± 7.3	0.040 ± 0.012
$2Na_2O{\cdot}3SiO_2$	0.0129 ± 0.0001	0.93	702	30 ± 15	0.068 ± 0.056
$CaO{\cdot}SiO_2$	0.106 ± 0.022	1.85	1038	50 ± 25	0.106 ± 0.022
$MgO{\cdot}SiO_2$	0.11 ± 0.01	2.5	1039	–	0.11 ± 0.01

k_1, k_2, and k_3 were calculated. An exponential increase in the magnitude of k_3 with modifying cation potential was initially observed but this trend did not consider the effects of varying glass transition temperature between glasses with different modifying cations. Utilizing previous work by Brandriss and Stebbins [58], the van't Hoff equation was used to normalize each glass to a single glass transition temperature, allowing measurements of k_3 for different glass compositions to be compared by eliminating the dependence of k_3 on thermal history. The resulting values for k_3 normalized to a glass transition temperature of 1039 K indicate that the disproportionation constant increases with cation potential.

Fits of anisotropic cross sections of the ^{29}Si 2D MAF spectrum also allowed the nuclear shielding parameters for $Q^{(1)}$ to be determined and applied to better understand the nuclear shielding tensor parameters for each $Q^{(n)}$-species in the $MgO \cdot SiO_2$ glass. The observed $\zeta^{(2)}$ and $\zeta^{(3)}$ values were consistent with trends reported in a previous MAF study [13], where the magnitude of ζ is observed to decrease as the cation potential increases. Based on results of Grimmer and coworkers [50,51], this trend of ζ versus cation potential indicates the increased ability of smaller more highly charged cations, such as Mg^{2+}, to withdraw electron density from the ^{29}Si nucleus as the Si–NBO bond length increases, ultimately approaching a bridging Si—O—Si bond. Future investigations using NMR techniques that rely on differences in the anisotropic lineshapes to better resolve multiple $Q^{(n)}$ sites of glasses with larger modifying cation potential than Mg^{2+} are expected to be problematic since, as the modifying cation potential increases, ζ for each $Q^{(n)}$ decreases and the nuclear shielding tensor parameters for each $Q^{(n)}$-species are increasingly similar.

Acknowledgements

The authors wish to thank Prof. George Papatheodorou and Mr. Nektarios Nasikas at ICEHT-FORTH in Patras, Greece, for the help in the preparation of glass samples. This material is based upon a work supported in part by the National Science Foundation. Any opinions, findings and conclusions or recommendations expressed in this material are those of the author(s) and do not necessarily reflect the views of the National Science Foundation (NSF).

Appendix A. Thermodynamic model

In a glass with composition $\alpha MO \cdot (1-\alpha)SiO_2$, we assume that the following anionic equilibria are present in the melt:

$$2Q^{(n)} \rightleftharpoons Q^{(n-1)} + Q^{(n+1)}, \tag{A.1}$$

with

$$K_n = \frac{\mathcal{A}_{Q_{n-1}}\mathcal{A}_{Q_{n+1}}}{\left(\mathcal{A}_{Q_n}\right)^2}, \tag{A.2}$$

and

$$2Q^{(0)} \rightleftharpoons 2Q^{(1)} + (O)^{2-}, \tag{A.3}$$

with

$$K_0 = \frac{\left(\mathcal{A}_{Q_1}\right)^2 \mathcal{A}_{(O)^{2-}}}{\left(\mathcal{A}_{Q_0}\right)^2}, \tag{A.4}$$

where $\mathcal{A}_Y$ is the activity of species Y. The activity of each species is related to its mole fraction, x_y, according to

$$\mathcal{A}_Y = \gamma_Y x_Y. \tag{A.5}$$

Substituting Eq. (A.5) into Eqs. (A.2) and (A.4) we obtain

$$k_n = \frac{\gamma_{Q_n}^2}{\gamma_{Q_{n-1}} \cdot \gamma_{Q_{n+1}}} \cdot K_n = \frac{x_{Q_{n-1}} \cdot x_{Q_{n+1}}}{x_{Q_n}^2}, \tag{A.6}$$

and

$$k_0 = \frac{\gamma_{Q_1}^2 \cdot \gamma_{(O)^{2-}}}{\gamma_{Q_0}^2} \cdot K_0 = \frac{x_{Q_1}^2 \cdot x_{(O)^{2-}}}{x_{Q_0}^2}. \tag{A.7}$$

The mole fractions used in calculating these equilibrium constants of our anionic thermodynamic equilibrium model requires

$$x_{Q_0} + x_{Q_1} + x_{Q_2} + x_{Q_3} + x_{Q_4} + x_{(O)^{2-}} = 1. \tag{A.8}$$

In ^{29}Si NMR experiment on the glass we measure the fraction of silicon in each of the five Q_n coordination states, y_{Q_n}, given by Eq. (11). Additional information is then needed to obtain the $(O)^{2-}$ mole fraction,

$$x_{(O)^{2-}} = \frac{n_{(O)^{2-}}}{n_{Q_0} + n_{Q_1} + n_{Q_2} + n_{Q_3} + n_{Q_4} + n_{(O)^{2-}}}, \tag{A.9}$$

as well as the $Q^{(n)}$ mole fractions,

$$x_{Q_n} = \frac{n_{Q_n}}{n_{Q_0} + n_{Q_1} + n_{Q_2} + n_{Q_3} + n_{Q_4} + n_{(O)^{2-}}}, \tag{A.10}$$

where n_{Q_n} is the total number of moles of the anionic species Q_n, and $n_{(O)^{2-}}$ is the total number of moles of the anion $(O)^{2-}$. Substituting Eq. (11) into the expressions above one obtains

$$x_{(O)^{2-}} = \frac{\left(n_{(O)^{2-}}/n_{Si}\right)}{y_{Q_0} + y_{Q_1} + y_{Q_2} + y_{Q_3} + y_{Q_4} + \left(n_{(O)^{2-}}/n_{Si}\right)}, \tag{A.11}$$

and

$$x_{Q_n} = \frac{y_{Q_n}}{y_{Q_0} + y_{Q_1} + y_{Q_2} + y_{Q_3} + y_{Q_4} + \left(n_{(O)^{2-}}/n_{Si}\right)}. \tag{A.12}$$

By combining the charge balance equation, given by

$$2n_{M^{2+}} = 4n_{Q_0} + 3n_{Q_1} + 2n_{Q_2} + n_{Q_3} + 2n_{(O)^{2-}}, \tag{A.13}$$

where $n_{M^{2+}}$ is the total number of moles of the cation M^{2+}, with the stoichiometric ratio

$$\frac{n_{M^{2+}}}{n_{Si}} = \frac{\alpha}{1-\alpha}, \tag{A.14}$$

one obtains

$$2\left(\frac{\alpha}{1-\alpha}\right) = 4\frac{n_{Q_0}}{n_{Si}} + 3\frac{n_{Q_1}}{n_{Si}} + 2\frac{n_{Q_2}}{n_{Si}} + \frac{n_{Q_3}}{n_{Si}} + 2\frac{n_{(O)^{2-}}}{n_{Si}}, \tag{A.15}$$

which can be rewritten as

$$\frac{n_{(O)^{2-}}}{n_{Si}} = \left(\frac{\alpha}{1-\alpha}\right) - 2y_{Q_0} - 1.5y_{Q_1} - y_{Q_2} - 0.5y_{Q_3}. \tag{A.16}$$

Substituting this expression into Eqs. (A.11) and (A.12) one obtains the expressions in Eqs. (13) and (14).

References

[1] S.R. Elliott, The Physics of Amorphous Materials, Longman Scientific & Technical, 1990, Essex CM20 2JE.
[2] A.K. Varshneya, Fundamentals of Inorganic Glasses, Academic Press Inc, 1250 Sixth Avenue, San Diego, CA 92101, 1994.

[3] B.O. Mysen, P. Richet, Silicate Glasses and Melts, Properties and Structure, Elsevier, 2005.
[4] W.H. Zachariasen, The atomic structure in glass, J. Am. Chem. Soc. 54 (1932) 3841–3851.
[5] A. Navrotsky, Energetics of silicate melts, in: J.F. Stebbins, P.F. McMillan, D.B. Dingwell (Eds.), Structure, Dynamics and Properties of Silicate Melts, Reviews in Mineralogy, vol. 32, Mineralogical Society of America, Washington, DC, 1995, pp. 121–143.
[6] P.C. Hess, Thermodynamic mixing properties and the structure of silicate melts, in: J.F. Stebbins, P.F. McMillan, D.B. Dingwell (Eds.), Structure, Dynamics and Properties of Silicate Melts, Vol. 32 of Reviews in Mineralogy, Mineralogical Society of America, Washington, DC, 1995, pp. 145–190.
[7] E.D. Lacy, A statistical model of polymerisation/depolymerisation relationship in silicate melts and glasses, Phys. Chem. Glasses 6 (5) (1965) 171–180.
[8] E. Lippmaa, M. Magi, A. Samoson, G. Engelhardt, A.-R. Grimmer, Structural studies of silicates by solid-state high-resolution ^{29}Si NMR, J. Am. Chem. Soc. 102 (1980) 4889–4893.
[9] K.A. Smith, R.J. Kirkpatrick, E. Oldfield, D.M. Henderson, High-resolution silicon-29 nuclear magnetic resonance spectroscopic study of rock-forming silicates, Am. Mineral 68 (1983) 1206–1215.
[10] G. Engelhardt, D. Michel, High-Resolution Solid-State NMR of Silicates and Zeolites, John Wiley & Sons, Chichester, 1987.
[11] J.F. Stebbins, Identification of multiple structural species in silicate glasses by ^{29}Si NMR, Nature 330 (1987) 465.
[12] P. Zhang, C. Dunlap, P. Florian, P.J. Grandinetti, I. Farnan, J.F. Stebbins, Silicon site distributions in an alkali silicate glass derived by two-dimensional ^{29}Si nuclear magnetic resonance, J. Non-Cryst. Solids 204 (1996) 294–300.
[13] M. Davis, D. Kaseman, S. Parvani, K. Sanders, P. Grandinetti, P. Florian, D. Massiot, $Q^{(n)}$-species distribution in K_2O $2SiO_2$ by ^{29}Si Magic Angle Flipping NMR, J. Phys. Chem. A 114 (17) (2010) 5503–5508.
[14] P. Zhang, P.J. Grandinetti, J.F. Stebbins, Anionic species determination in $CaSiO_3$ glass using two-dimensional ^{29}Si NMR, J. Phys. Chem. B 101 (20) (1997) 4004–4008.
[15] A. Bax, N.M. Szeverenyi, G.E. Maciel, Correlation of isotropic shifts and chemical shift anisotropies by two-dimensional Fourier-transform magic-angle hopping NMR spectroscopy, J. Magn. Reson. 52 (1983) 147.
[16] F. Press, R. Siever, Earch, Freeman, 1986.
[17] K. Fujino, S. Sasaki, Y. Takeuchi, R. Sadanaga, X-ray determination of electron distributions in forsterite, fayalite and tephroite, Acta Crystallogr. Sect. B Struct. Sci. 37 (1981) 513–518.
[18] A. G. Kalampounias, N. K. Nasikas, G. N. Papatheodorou, Glass formation and structure $MgSiO_3$–Mg_2SiO_4 pseudobinary system: From degraded networks to ioniclike glasses, J. Chem. Phys. 131.
[19] S. Sen, J. Tangeman, Evidence for anomalously large degree of polymerization in Mg_2SiO_4 glass and melt, Am. Miner. 93 (5–6) (2008) 946–949.
[20] S. Sen, H. Maekawa, G.N. Papatheodorou, Short-range structure of invert glasses along the pseudo-binary join $MgSiO_3$–Mg_2SiO_4: results from ^{29}Si and ^{25}Mg MAS NMR spectroscopy, J. Phys. Chem. B 113 (113) (2009) 15243–15248.
[21] M.A. Eastman, P.J. Grandinetti, Y.K. Lee, A. Pines, Double-tuned hopping-coil probe for dynamic-angle spinning NMR, J. Magn. Reson. 98 (1992) 333–341.
[22] M. Mehring, High resolution NMR spectroscopy in solids, Vol. 11, Springer-Verlag, Berlin, 1983.
[23] A.C. Kolbert, P.J. Grandinetti, M. Baldwin, S.B. Prusiner, A. Pines, Measurement of internuclear distances by switched angle spinning NMR, J. Phys. Chem. 98 (33) (1994) 7936–7938.
[24] R.R. Ernst, G. Bodenhausen, A. Wokaun, Principles of Nuclear Magnetic Resonance in One and Two Dimensions, Oxford, Oxford, , 1987.
[25] A. Bax, N.M. Szeverenyi, G.E. Maciel, Chemical shift anisotropy in powdered solids studied by 2D FT NMR with flipping of the spinning axis, J. Magn. Reson. 55 (1983) 494.
[26] P.J. Grandinetti, J.H. Baltisberger, A. Llor, Y.K. Lee, U. Werner, M.A. Eastman, A. Pines, Pure absorption-mode lineshapes and sensitivity in two-dimensional dynamic angle spinning NMR, J. Magn. Reson. A 103 (1993) 72–81.
[27] H.Y. Carr, E.M. Purcell, Effects of diffusion on free precession in nuclear magnetic resonance experiments, Phys. Rev. 94 (1954) 630–638.
[28] S. Meiboom, D. Gill, Modified spin-echo method for measuring nuclear relaxation times, Rev. Sci. Instrum. 29 (1958) 688.
[29] R. Siegel, T.T. Nakashima, R.E. Wasylishen, Application of multiple-pulse experiments to characterize broad NMR chemical-shift powder patterns from spin-1/2 nuclei in the solid state, J. Phys. Chem. B 108 (2004) 2218–2226.
[30] J.W. Wiench, V.S.Y. Lin, M. Pruski, ^{29}Si NMR in solid state with CPMG acquisition under MAS, J. Mag. Res. 193 (2008) 233–242.
[31] I. Hung, A.J. Rossini, R.W. Schurko, Application of Carr–Purcell–Meiboom–Gill pulse sequence for the acquisition of solid-state NMR spectra of spin-1/2 nuclei, J. Phys. Chem. A 108 (2004) 7112–7120.
[32] F.H. Larsen, I. Farnan, ^{29}Si and ^{17}O (Q)CPMG-MAS solid-state NMR experiments as an optimum approach for half-integer nuclei having long t_1 relaxation times, Chem. Phys. Lett. 357 (2002) 403–408.
[33] J.Z. Hu, R.A. Wind, Sensitivity-enhanced phase-corrected ultra-slow magic angle turning using multiple-echo data acquisition, J. Magn. Reson. 163 (2003) 149–162.
[34] D. Sakellariou, J.-F. Jacquinot, T. Charpentier, 2D correlation spectra of isotropic and anisotropic ^{29}Si chemical shifts in crystalline and amorphous natural abundance materials under very slow sample rotation, Chem. Phys. Lett. 411 (2005) 171–174.
[35] K. Dey, J. Ash, N. Trease, P. Grandinetti, Trading sensitivity for information: CPMG acquisition in solids, J. Chem. Phys. 133 (2010), 05401–01–054501–10.
[36] J.T. Ash, N.T. Trease, P.J. Grandinetti, Separating chemical shift and quadrupolar anisotropies via multiple-quantum nmr spectroscopy, J. Am. Chem. Soc. 130 (2008) 10858–10859.
[37] R.K. Harris, E.D. Becker, S.M.C.D. Menezes, P. Grangerd, R.E. Hoffman, K.W. Zilm, Further conventions for NMR shielding and chemical shifts, IUPAC recommendations 2008, Inorg. Chem. 3 (2008) 41–56.
[38] M. Baks, J.T. Rasmussen, N.C. Nielsen, SIMPSON: a general simulation program for solid-state NMR spectroscopy, J. Magn. Reson. 147 (2000) 296–330.
[39] C.R. Masson, An approach to the problem of ionic distribution in liquid silicates, Proc. R. Soc. London Ser. A 287 (1965) 201–221.
[40] C.R. Masson, I.B. Smith, S.G. Whiteway, Activities and ionic distribution in liquid silicates: application of polymer theory, Can. J. Chem. 48 (1970) 1456–1464.
[41] D.R. Gaskell, The thermodynamic properties of the masson polymerization models in liquid silicates, Metall. Trans. 4 (1973) 185–192.
[42] D.R. Gaskell, Activities and free energies of mixing in binary silicate melts, Metall. Trans. 8B (1977) 131–145.
[43] S.J. Gurman, Bond ordering in silicate glasses: a critique and a re-solution, J. Non-Cryst. Solids 125 (1990) 151.
[44] W.G. Dorfeld, Structural thermodynamics of alkali silicates, Phys. Chem. Glasses 29 (1988) 179.
[45] N. Weiden, H. Rager, The chemical shift of the ^{29}Si nuclear magnetic-resonance in a synthetic single-crystal of Mg_2SiO_4, Z. Naturforsch. A A J. Phys. Sci. 40 (1985) 126–130.
[46] S.E. Ashbrook, L. Le Polles, C.J. Pickard, A.J. Berry, S. Wimperis, I. Farnan, First-principles calculations of solid-state ^{17}O and ^{29}Si NMR spectra of Mg_2SiO_4 polymorphs, Phys. Chem. Chem. Phys. 9 (2007) 1587–1598.
[47] P.C. Hess, Polymer model of silicate melts, Geochim. Cosmochim. Acta 35 (1971) 289–306.
[48] C.R. Masson, Ionic equilibria in liquid silicates, J. Am. Ceram. Soc. 51 (1968) 134–143.
[49] S.E. Ashbrook, A.J. Berry, W.O. Hibberson, S. Steuernagel, S. Wimperis, High-resolution O-17 MAS NMR spectroscopy of forsterite (alpha-Mg2SiO4) wadsleyite (beta-Mg2SiO4), and ringwoodite (gamma-Mg2SiO4), Am. Miner. 90 (11–12) (2005) 1861–1870.
[50] A.-R. Grimmer, E.F. Gechner, G. Molgedey, High resolution ^{29}Si NMR in solid silicates. correlations between shielding tensor and Si—O bond length, Chem. Phys. Lett. 77 (1981) 331–335.
[51] A.-R. Grimmer, Correlation between individual Si—O bond lengths and the principal values of the ^{29}Si chemical-shift tensor in solid silicates, Chem. Phys. Lett. 119 (1985) 416–420.
[52] E.J.W. Whittaker, R. Muntus, Ionic radii for use in geochemistry, Geochim. Cosmochim. Acta 34 (1970) 945–956.
[53] W.J. Malfait, W.E. Halter, Y. Morizet, B.H. Meier, R. Verel, Structural control on bulk melt properties: single and double quantum ^{29}Si NMR spectroscopy on alkali-silicate glasses, Geochim. Cosmochim. Acta 71 (2007) 6002–6018.
[54] H. Maekawa, T. Maekawa, K. Kawamura, T. Yokokawa, The structural groups of alkali silicate glasses determined from ^{29}Si MAS-NMR, J. Non-Cryst. Solids 127 (1991) 53–64.
[55] C. Larson, J. Doerr, M. Affatigato, S. Feller, D. Holland, S. M.E., A ^{29}Si MAS NMR study of silicate glasses with a high lithium content, J. Phys. Condens. Matter 18 (2006) 11323–11331.
[56] V.P. Zakaznova-Herzog, W.J. Malfait, F. Herzog, W.E. Halter, Quantitative Raman spectroscopy: principles and application to potassium silicate glasses, J. Non-Cryst. Solids 353 (2007) 4015–4028.
[57] E. Schneider, V. Mastelaro, E. Zanotto, B. Shakhmatkin, N. Vedishcheva, A. Wright, H. Panepucci, Q^n distribution in stoichiometric silicate glasses: thermodynamic calculations and ^{29}Si high resolution NMR measurements, J. Non-Cryst. Solids 325 (2003) 164–178.
[58] M.E. Brandriss, J.F. Stebbins, Effects of temperature on the structures of silicate liquids: ^{29}Si NMR results, Geochim. Cosmochim. Acta 52 (1988) 2659–2669.
[59] J.B. Murdoch, J.F. Stebbins, I.S.E. Carmichael, High-resolution ^{29}Si NMR study of silicate and aluminosilicate glasses: the effect of network-modifying cations, Am. Mineral 70 (1985) 332–343.
[60] J.F. Stebbins, Effects of temperature and composition on silicate glass structure and dynamics: Si-29 NMR results, J. Non-Cryst. Solids 106 (1988) 359–369.
[61] C.T. Moynihan, A.J. Easteal, J. Wilder, Dependence of the glass transition on heating and cooling rate, J. Phys. Chem. 78 (1974) 2673–2677.
[62] W.J. Malfait, V.P. Zakaznova-Herzog, W.E. Halter, Quantitative Raman spectroscopy: high-temperature speciation of potassium silicate melts, J. Non-Cryst. Solids 353 (2007) 4029–4042.